ORIGINAL ARTICLE

Monodispersed biodegradable microparticles with wrinkled surface coated with silver nanoparticles for catalytic degradation of organic toxins

Minjun Chen[1] · Guido Bolognesi[1,2] · Robina Begum[1,3] · Zahoor H. Farooqi[1,3] · Goran T. Vladisavljević[1]

Abstract

Microfluidic fabrication of monodisperse microgels for biomedical, nanotechnological, environmental, and catalytic applications has become the subject of growing interest. In this work, monodisperse polyethylene glycol diacrylate [P(EGDA)] microgel particles were fabricated using a CNC-milled microfluidic device with a Lego-inspired interlocking mechanism. Silver nanoparticles (AgNPs) were synthesised and stabilised in situ on the wrinkled surface of the microgel particles using $AgNO_3$ as a metal precursor and $NaBH_4$ as a reductant. The loading of AgNPs (7.5 wt%) on microgel beads was confirmed by energy-dispersive X-ray spectroscopy, X-ray diffraction, and thermogravimetric analysis. Surface wrinkles were found to be a useful morphological feature acting as reservoirs for the accumulation of AgNPs. Ag–P(EGDA) hybrid polymer particles were shown to be an efficient catalyst for the reduction of 4-nitrophenol (4NP) into 4-aminophenol (4AP) by sodium borohydride at room temperature. After 40 min, 0.08 M 4NP was completely converted into 4AP using 2.1 mg/mL of Ag–P(EGDA) catalytic particles, and the reaction followed a pseudo-first-order kinetics. The apparent rate constant increased from 0.0142 to 0.117 min^{-1} when the loading of catalytic particles increased from 1.7 to 2.50 mg/mL indicating that the reduction is occurring on the catalyst surface according to the Langmuir–Hinshelwood model. Ag–P(EGDA) hybrid microgel was a potent and recyclable catalyst for room-temperature degradation of methylene blue (MeB) by $NaBH_4$. At the Ag–P(EGDA) loading of 2.0 mg/mL, 25 μM of MeB was completely degraded in 6 min. Composite Ag–P(EGDA) microgel beads can be used as an eco-friendly and easily recoverable catalyst for the transformation of other organic pollutants into useful chemicals.

Keywords Droplet microfluidics · Monodisperse microgel particles · Hybrid microgel particles · Catalytic applications

1 Introduction

Microgels are hydrophilic crosslinked polymeric microparticles which are gaining increasing attention in biomedical [1], environmental [2], and nanotechnological [3] fields, due to their softness, versatility of chemical structure, biomimetic properties, and high biocompatibility. Depending on environmental conditions, microgel particles can get swelled by absorption of water or shrunk upon removal of water from their polymeric network. This high and stimuli-dependent water absorption capacity makes them desirable for a myriad of applications, especially in biology and biomedicine [4, 5]. They are also being used as micro-reactors and templates for synthesis and stabilisation of inorganic nanoparticles [6, 7]. Microgel particles with highly uniform and tunable sizes are required in most biomedical applications because their efficiency, loading capacity, and stability depend upon their size distribution. Microgels with uniform size can be manufactured by surfactant-free radical precipitation polymerisation [8–11], but the particles obtained by this technique are smaller than 1 μm, and ultracentrifugation is needed for their recovery from the reaction mixture. In recent years, droplet microfluidics have been widely used for

✉ Zahoor H. Farooqi
 zhfarooqi@gmail.com; zahoor.chem@pu.edu.pk;
 Z.Farooqi@lboro.ac.uk

✉ Goran T. Vladisavljević
 G.Vladisavljevic@lboro.ac.uk

1 Department of Chemical Engineering, Loughborough University, Loughborough LE11 3TU, UK

2 Department of Chemistry, University College London, London WC1H 0AJ, UK

3 School of Chemistry, University of the Punjab, New Campus, Lahore 54590, Pakistan

جامعة قطر
QATAR UNIVERSITY

🜋 Springer

the room-temperature production of monodisperse microgel particles with a diameter in the range of 10–1000 μm [12, 13]. Microfluidic fabrication methods offer fine-tuning of the size, internal structure, and morphology of microgel particles, and their swelling and deswelling kinetics can be manipulated by introducing spherical voids within the polymer matrix using latex particles as templates [14].

Poly(ethylene glycol) diacrylate (PEGDA) is one of the most widely used polymers for microfluidic fabrication of microgels due to its easy functionalization and copolymerization, low toxicity, availability over a wide range of molecular weights, and crosslinking ability under UV-irradiation [15–17]. Celletti et al. [18] have reported synthesis of peptide entrapped P(EGDA) microgels using flow focusing PDMS chip for selective capture of biomolecules in a complex medium. The microgel system has the potential to be used for the detection of a variety of proteins in complex medium. Liu et al. [19] have successfully loaded core–shell quantum dots with CdSe core and ZnS shell into the network of P(EGDA) to obtain a hybrid material for suspension assay. Lewis et al. [20] have loaded tobacco mosaic virus (TMV) functionalized palladium (Pd) nanoparticles into P(EGDA) microparticles via a microfluidic method for catalytic conversion of Cr(IV) into Cr(III) in aqueous phase. Kang et al. [21] have immobilised polyvinyl pyrrolidone-stabilised Pd nanoparticles on P(EGDA) microbeads and used the resulting hybrid material as a catalyst for the reduction of 4-nitrophenol (4NP) in water. Kim et al. [22] have incorporated and agglomerated pre-synthesised silver nanocubes within P(EGDA) particles and used these hybrid microgels for surface-enhanced Raman scattering detection of aspirin in blood. The hybrid system can be used for both qualitative and quantitative analysis of small molecules present in biological fluids.

Due to their antibacterial, antifungal, and antiviral activities, Ag-polymer hybrid materials have been widely reported for biomedical applications including wound healing, tissue engineering, cancer treatment, dental materials preparation, vascular grafting, bio-sensing, and diagnostic processing [23–26]. The polymeric material not only stabilises silver nanoparticles against aggregation but also controls the release of Ag^+ ions to mitigate cytotoxicity [27, 28].

In this study, we have synthesised silver nanoparticles (NPs) on a wrinkled surface of monodispersed polyethylene glycol diacrylate [P(EGDA)] microparticles produced via Lego-inspired glass capillary microfluidic device. For the first time, monodispersed micron-sized P(EGDA) microgel particles have been used as microporous support for the fabrication and stabilisation of silver NPs. The produced Ag–P(EGDA) hybrid microgels were investigated for their catalytic activity towards the reduction of 4NP and methylene blue (MeB) from their aqueous solutions. P(EGDA) microgel stabilises silver NPs via donor–acceptor interactions between carbonyl groups of P(EGDA) and zerovalent silver [29] and provides a corrugated surface to maximise the loading of silver NPs. In addition, due to their size in the micrometre range, new catalytic particles can easily be recovered from the reaction mixture, unlike nanometre-sized hybrid particles used in previous studies [30].

2 Experimental

2.1 Materials

Poly(ethylene glycol) diacrylate (PEGDA) with $M_w = 700$ g/mol, 2-hydroxy-40-(2-hydroxyethoxy)-2-methyl-propiophenone (Darocur 2959), silver nitrate (99%), 4-nitrophenol (98%), and sodium borohydride (98%) were obtained from Sigma-Aldrich, UK. MeB was acquired from Fisher Bio-Reagents™ (Fisher Scientific, UK). XIAMETER™ PMX-200 Silicone Fluid, 100 cSt, and XIAMETER™ RSN-0749 Resin (50/50 mixture of trimethylsiloxysilicate and cyclomethicone) were obtained from Dow Chemical, USA. All chemicals were used as received without any further purification. All solutions were prepared using ultrapure water purified via the Milli-Q Plus 185 (Millipore) system.

2.2 Synthesis of pure P(EGDA) particles

Water-in-oil (W/O) emulsion was generated by 3D counter-current flow focusing in a Lego-inspired glass capillary device, as presented in Fig. 1A [31]. A complete description of the microfluidic procedure and experimental setup has been already provided in our publications [32, 33]. Briefly, the dispersed phase was introduced through the outer capillary into a pulled coaxially aligned inner capillary. The dispersed phase jet was broken into droplets due to the high speed of the continuous phase at the inlet of the internal capillary. Droplet production was monitored with a Basler camera (Aca720–520uc, Germany) attached to an inverted microscope.

The continuous phase was XIAMETER™ PMX-200 silicone oil having 3.50 wt% RSN-0749 surfactant, and the dispersed phase was composed of 48 wt% P(EGDA) macromer and 2 wt% Darocur 2959 (Irgacure 2959) photoinitiator dissolved in Milli-Q water. The flow rates of the continuous phase and dispersed phase in the microfluidic device were kept constant at 0.80 mL/h and 0.16 mL/h, respectively, using the Harvard Apparatus 11 Elite syringe pumps (Biochrom Ltd, UK). Both phases were brought from SGE gas-tight glass syringes of 10 mL (Sigma-Aldrich, UK) linked to the device via polyethylene medical tubing (ID 0.86 mm, OD 1.52 mm, Smiths Medicals, Luton, UK). The dispersed phase tubing was shielded by aluminium foil to avoid pre-mature P(EGDA) polymerisation. The droplets
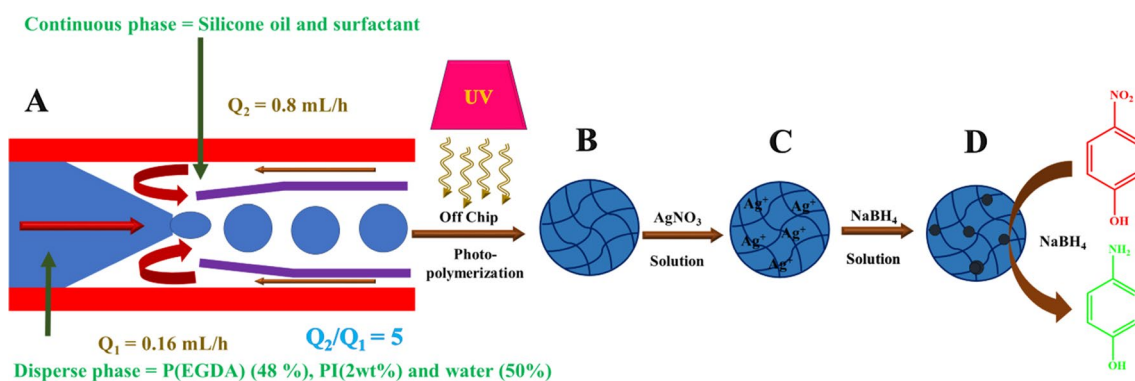
Fig. 1 An overview of the microfluidic production of P(EGDA) beads for in-situ synthesis of Ag nanoparticles and their application as catalyst for the reduction of 4-nitrophenol in aqueous medium: A micro-fluidic strategy for droplet generation; B pure P(EGDA) microgel; C P(EGDA) microgel loaded with Ag$^+$ ions; and D catalytic conversion of 4NP into 4AP by hybrid Ag–P(EGDA) microgel

produced in the microfluidic device were collected in a Petri dish prefilled with the dispersion medium. After production, the Petri dish was placed under a UV lamp (UVAHAND 250GS Dr. Hönle AG, Gilching, Germany) for 6.5 min to cure the droplets, Fig. 1B. The UV light wavelength was 365–395 nm, and the irradiance was 750 W/m^2, as measured by a radiometer (365.0 nm, VLX-3W). The resulting microgel beads were washed 6–7 times using acetone and deionised water to eliminate the oil phase.

2.3 Synthesis of Ag–P(EGDA) hybrid particles

P(EGDA) particles were used as microreactors for the production and stabilisation of silver NPs. For this purpose, 0.75 g of P(EGDA) beads were dispersed in 24.5 mL of 16.33 mM silver nitrate solution, and the suspension was agitated overnight to allow diffusion of AgNO$_3$ within the polymer network. The suspension was then centrifuged at 4000 rpm and 4 °C, the supernatant was removed, and P(EGDA) beads loaded with AgNO$_3$ (Fig. 1C) were re-dispersed in 20 mL of deionised water. Then, 5 mL of freshly prepared sodium borohydride solution (0.0378 g/mL) was added dropwise into the dispersion, and the resulting mixture was agitated at room temperature for 30 min. Finally, the suspension was centrifuged in a Fisherbrand™ GT2 Expert centrifuge (Fisher Scientific, UK) at room temperature and 4000 rpm. After removing the supernatant, the prepared Ag–P(EGDA) hybrid beads (Fig. 1D) were stored in the dark before being used.

2.4 Characterisation of P(EGDA) beads and Ag–P(EGDA) hybrid beads

Bright-field images of W/O emulsion droplets and P(EGDA) microgels were captured by a CCD camera (Retiga 6000.0, Canada) interfaced with a computer having Q-capture software. The surface morphology of pure P(EGDA) particles and Ag–P(EGDA) hybrid particles was studied by a field emission SEM (JEOL, JSM 7800F, Japan) working at an accelerating voltage of 5.0 kV. A UV–vis spectrophotometer (NanoDrop™ One/OneC, Thermo Fisher Scientific, USA) was used to monitor the progress of 4NP and MeB reduction in the wavelength range of 230–530 nm and 350–850 nm, respectively. X-ray diffraction analysis was carried out by using an XRD instrument D2 phaser (Bruker UK Limited, UK). A TGA 550 instrument (TA instruments, USA) was employed to monitor the weight loss of dried particles of P(EGDA) beads and Ag–P(EGDA) hybrid beads (12.0 mg each) under N$_2$ atmosphere in the range of 20–600 °C at a heating rate of 10.0 °C/min.

2.5 Catalysis using Ag–P(EGDA) hybrid beads

4-nitrophenol solution (1.0 mM, 2.0 mL), freshly prepared sodium borohydride solution (100 mM, 2.0 mL), and different amounts of Ag–P(EGDA) hybrid beads (40 to 60 mg) were added into a flask filled with 20 mL of water, and the reaction mixture was subjected to gentle stirring at room temperature. Every 3 min, 2.5 mL of the solution was taken in a cuvette, and spectra were recorded in the wavelength range of 230–530 nm. Similarly, a mixture of MeB solution (31.3 μM, 20.0 mL), freshly prepared sodium borohydride solution (145.4 mM, 5.0 mL), and Ag–P(EGDA) hybrid beads (50 mg) was stirred to achieve

the degradation of MeB. 2.5 mL of the reaction mixture was taken at regular time intervals, and their absorption spectra were measured in the 350–850 nm range to check the reaction progress. All controlled experiments were performed under similar reaction conditions.

3 Results and discussion

3.1 Fabrication and characterisation of P(EGDA) and Ag–P(EGDA) microgels

Optical microscopy images of W/O emulsion droplets before UV curing are shown in Fig. 2A. The droplets are highly monodisperse with a CV value of 1.2% (Table 1) and barely visible due to a similar refractive index of the inner phase (1.42) [34] and pure silicone oil (1.40) [32].

Under UV light, the acrylate end-groups of PEGDA-700 polymerised to form crosslinking nodes connected by PEG backbones. Microscopic images of P(EGDA) microgels in oil phase are shown in Fig. 2B. Nearly monodisperse P(EGDA) microgel beads were obtained with a CV of 1.7%. This excellent size uniformity of the microgel particles is only possible by microfluidic technology. Accurate size control is crucial for biomedical and environmental applications because many properties of hydrogel particles such as swelling behaviour, drug release kinetics, and adsorption properties are size-dependent. The size of P(EGDA) particles was reduced from 220 to 137 μm during crosslinking, mainly due to the expulsion of water from the droplets during crosslinking. Also, before crosslinking PEGDA-700 molecules interact only by weak van der Waals forces which keep them at least 0.30–0.40 nm apart [35], while after polymerisation, covalent bonds with a length of ~ 0.15 nm [36] are formed between PEGDA-700 molecules.

P(EGDA) microgel particles swell in water since P(EGDA) is a hydrophilic polymer due to the presence of ethoxy groups. Therefore, the diameter of P(EGDA) particles increased from 137 to 158 μm after their transfer from silicone oil (Fig. 2B) to water (Fig. 2C). A high

Table 1 The values of average diameter, standard deviation, and coefficient of variation of W/O droplets, P(EGDA) beads in the oil phase, and P(EGDA) beads in the aqueous phase

Parameter	W/O droplets	P(EGDA) beads in oil	P(EGDA) beads in water
Count number	54	54	55
Average diameter (μm)	220	137	158
Standard deviation (μm)	2.6	2.3	2.6
Coefficient of variation (%)	1.2	1.7	1.6

magnification image of washed P(EGDA) particle in the inset of Fig. 2C shows that P(EGDA) beads have been successfully produced with surface irregularities, which is a useful feature that can allow higher loading of silver NPs. Figure 2B and C reveal that particles have a narrow size distribution in both oil and water phases.

The average size and size distribution of P(EGDA) particles depend upon the orifice size of the inner capillary, the flow rates of the continuous and dispersed phases and their composition have been optimised in our previous work to obtain monodisperse P(EGDA) particles with well-defined spherical shape and porosity [32].

The resulting P(EGDA) microgel beads were loaded with silver ions using silver nitrate as a source of metal ions. The beads suspended in silver nitrate solution were stirred overnight to maximise the mass transfer of silver ions from the bulk solution into the liquid phase filling the interstitial space of the P(EGDA) polymeric network. The silver ions remaining in the bulk solution (outside the polymer network) were removed by centrifugation of the suspension and separation of the supernatant from the settled beads. Dropwise addition of newly prepared NaBH$_4$ solution into dispersion of P(EGDA) beads changed the colour of the reaction mixture to brownish, which was a clear sign of the formation of silver NPs within the beads by reduction of silver ions with borohydride: $Ag^+ + 2BH_4^- \rightarrow Ag + H_2 + B_2H_6$. However, the leaching of silver ions into the bulk solution before their reduction on P(EGDA) beads cannot be totally ignored.
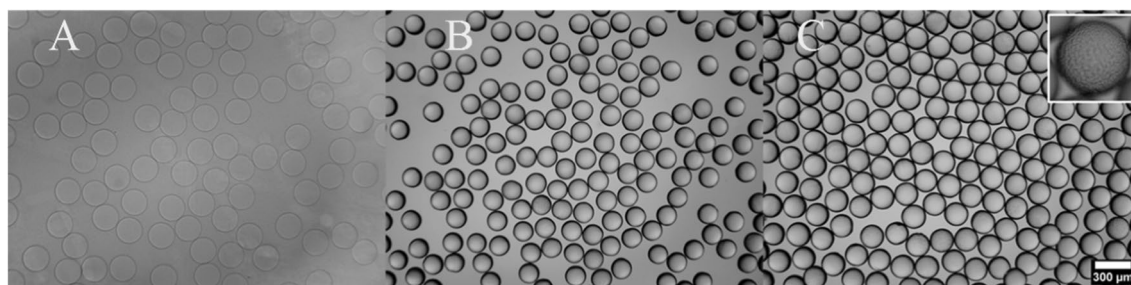

Fig. 2 Optical microscopic images of **A** W/O droplets, **B** P(EGDA) microgel particles in silicone oil, and **C** P(EGDA) microgel particles in aqueous medium

Therefore, a reduction of Ag$^+$ ions outside the beads may be expected. If Ag$^+$ ions are reduced outside the polymer network to form silver NPs in the bulk aqueous phase, they can easily be agglomerated before adhesion to the surface of P(EGDA) beads. NaBH$_4$ was added in excess to achieve a complete reduction of silver ions loaded into P(EGDA) beads.

The morphological studies of P(EGDA) beads and their composite were carried out by SEM. The SEM images of P(EGDA) microgels and Ag–P(EGDA) hybrid microgels at different magnifications are presented in Figs. 3 and 4,
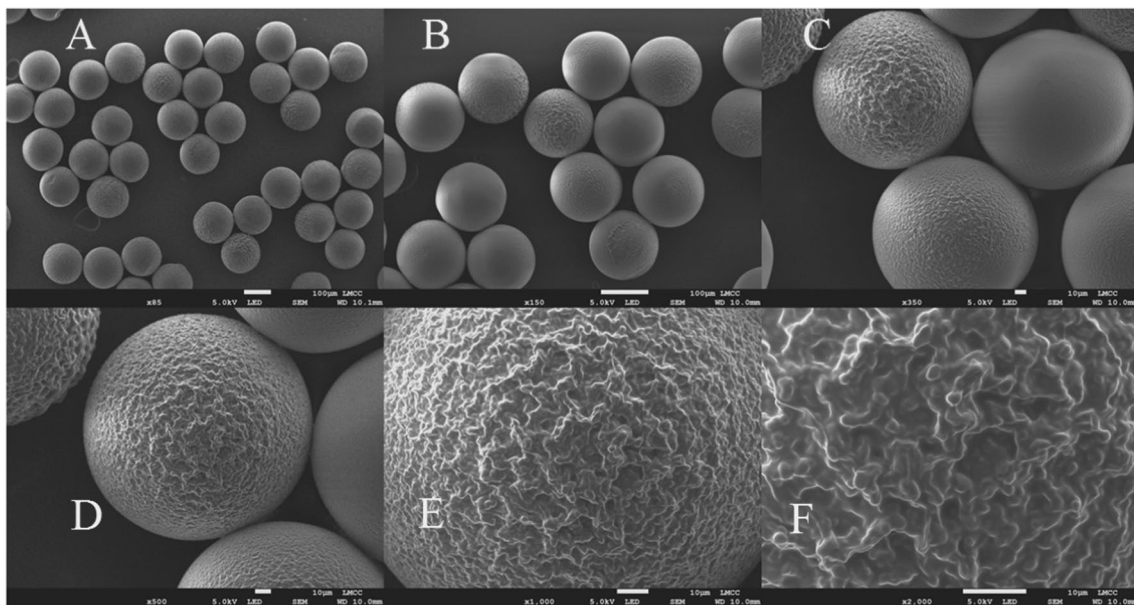
Fig. 3 SEM images of P(EGDA) particles at various magnifications demonstrating their size, shape, and surface morphology. The scale bar is 100 μm (**A** and **B**) and 10 μm (**C–F**)
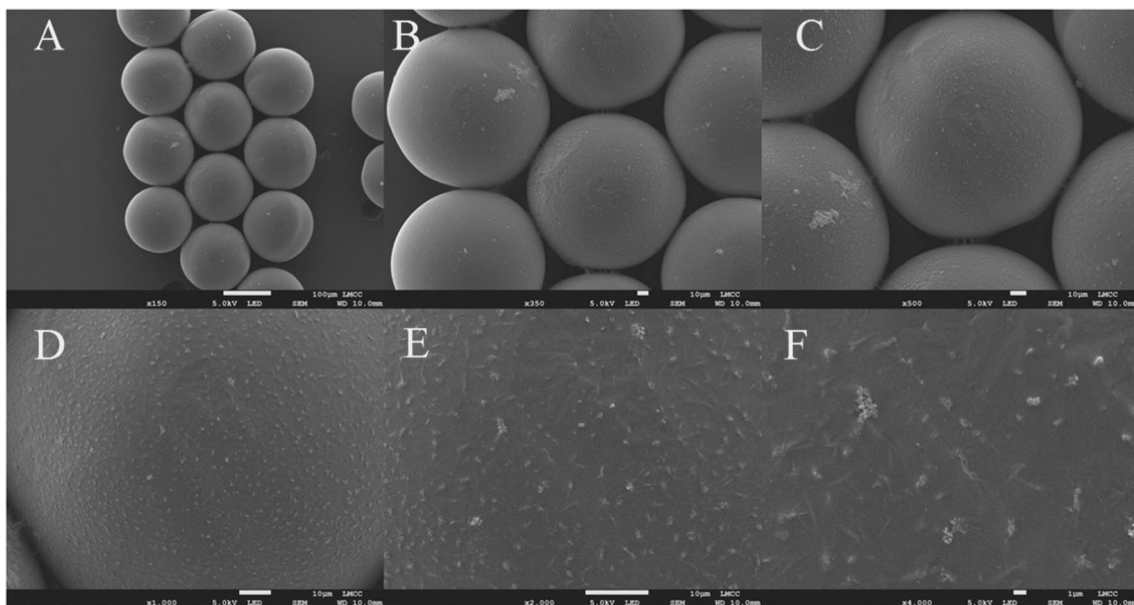
Fig. 4 SEM images of Ag–P(EGDA) hybrid particles at various magnifications indicating their size, shape, and surface morphology. The value of the scale bar is 100 μm (**A**), 10 μm (**B–E**), and 1 μm (**F**). Aggregates of silver NPs can be clearly seen on the polymer surface at higher magnifications

respectively. As shown in Fig. 3A–D, P(EGDA) beads are perfectly spherical without any unwanted bridges between individual beads. A rough surface morphology which can be seen in Fig. 3E–F was obtained by creating a non-uniform concentration of dissolved oxygen within the aqueous phase droplets during photo-polymerisation. It led to faster polymerisation of the interior of the droplets compared to the surface region and spontaneous surface wrinkling. The lack of visible pores on the surface is consistent with a reported mesh size of PEGDA-700 hydrogel of ~ 1.5 nm [37].

There is no change in the shape and size of beads upon synthesis of silver NPs within the P(EGDA) matrix, as reflected in Fig. 4A–C. However, the loading of silver nanoparticles into the P(EGDA) microgel beads increased the smoothness of their surface which may be attributed to the filling of pores with silver nanoparticles. It was observed earlier that inorganic nanoparticles embedded within a host polymer may play the role of porosity reducer [38]. Moreover, wrinkles on the surface of polymer beads act as cavities to accommodate silver nanoparticles. So, the smoothness of the surface of beads increases due to the filling of the cavities of beads by AgNPs. Wrinkles act as catchers for silver nanoparticles to make a highly stable Ag–P(EGDA) hybrid system. Kim et al. [39] reported that the loading of Fe_3O_4 nanoparticles on the wrinkled surface of polymer beads was higher than that on the smooth surface, despite the same diameter and chemical composition of both surfaces. However, in our case, some metal particles can be seen as white spots in SEM images (Fig. 4). These agglomerates are too large to fill the cavities and are present on the smooth surface of the P(EGDA) beads suggesting that two independent phenomena occurred during synthesis of AgNPs: some Ag nanoparticles that can be seen as white floccules on the P(EGDA) SEM images, have been formed in the bulk aqueous phase and agglomerated in water before being deposited on the polymer surface. However, most Ag nanoparticles have been directly formed on the surface, and they cannot clump together after formation because they are nonmobile and cannot move through the polymer network. Such non-agglomerated nanoparticles cannot be seen on SEM images, and they may lead to the smoother surface of hybrid beads. Interestingly, silver nanoparticles present both in the wrinkles and smooth surface of the beads were found stable which may be attributed to the strong interaction between silver metal and P(EGDA) due to charge transfer from oxygen (O) of carbonyl groups of P(EGDA) to silver nanoparticles. Dong et al. [40] proved this type of interaction using XPS and reported that this is the main cause of the stability of silver nanoparticles in the vicinity of microgels containing carbonyl functionalities.

EDX combined with SEM was used to check the presence of silver NPs on the beads and to find the elemental composition of the Ag–P(EGDA) system. EDX silver mapping shown in Fig. 5A and B indicates that silver NPs are present on the surface of the microgel particles, and the silver content is 2.7 wt%. The appearance of the absorbance peak at 3 keV suggests the presence of zerovalent silver in the hybrid microgel system, Fig. 5C.

Most of the Ag NPs were found on the surface/outer region of the P(EGDA) beads. It was confirmed by taking the SEM images of Ag–P(EGDA) beads after cutting different microgel particles with a sharp knife and performing silver mapping again. Most of the inner area of the beads was found free of silver particles, and only a limited number of very small silver NPs were detected in the inner region, as shown in Fig. S1 (A and B) (Supporting Information). Similar behaviour was found when silver NPs were deposited onto poly(methyl methacrylate) (PMMA) beads by microwave-assisted coating [41].

The loading of silver NPs on the P(EGDA) beads was also proved by XRD analysis of both P(EGDA) and Ag–P(EGDA) beads (Fig. 6). Two wide peaks at 2θ values of 10–33° and 34–47° are related to P(EGDA) polymer and were observed in both cases. No sharp peak was observed in the 2θ range of 36–80° in the XRD pattern of pure P(EGDA) beads while four peaks at 2θ values of 38.28°, 44.36°, 64.11°, and 77.79° can be clearly observed in the XRD of Ag–P(EGDA) beads which may be associated to the (111), (200), (220), and (311) crystalline planes of fcc (face-centred cubic) crystals of Ag [42] (Inset of Fig. 6). The width of the peak at 2θ value of 38.28° was used for evaluation of the crystallite size of silver NPs loaded on P(EGDA) beads using the Scherer equation, and its value was found to be 9.4 nm.

TGA of P(EGDA) and Ag–P(EGDA) systems was performed to investigate the thermal stability of both samples and further confirm the presence of Ag NPs in hybrid microgels. Figure 7 shows the percentage of P(EGDA) and Ag–P(EGDA) sample weights as a function of temperature over the range of 19–600 °C.

The TGA curves for both samples can be divided into three regions (I, II, and III) depending upon the extent of weight loss on heating, as shown in Fig. 7. In Region I (T ≤ 160 °C for pure beads and T ≤ 280 °C for hybrid beads), the weight loss occurred due to removal of interstitial water by evaporation. Hybrid beads showed much smaller weight loss in the region between 160 and 280 °C, probably because the layer of silver NPs provided a diffusional barrier to the thermal evaporation of water.

The weight loss in Region II (160 °C ≤ T ≤ 320 °C for pure beads and 280 °C ≤ T ≤ 380 °C for hybrid beads) may be due to the degradation of carbonyl groups of P(EGDA) and Ag–P(EGDA) microgels. Interestingly, the loading of the P(EGDA) polymer network with silver NPs increased the thermal stability of the polymer, as reflected in the shift of the TGA curve of Ag–P(EGDA) microgel towards higher
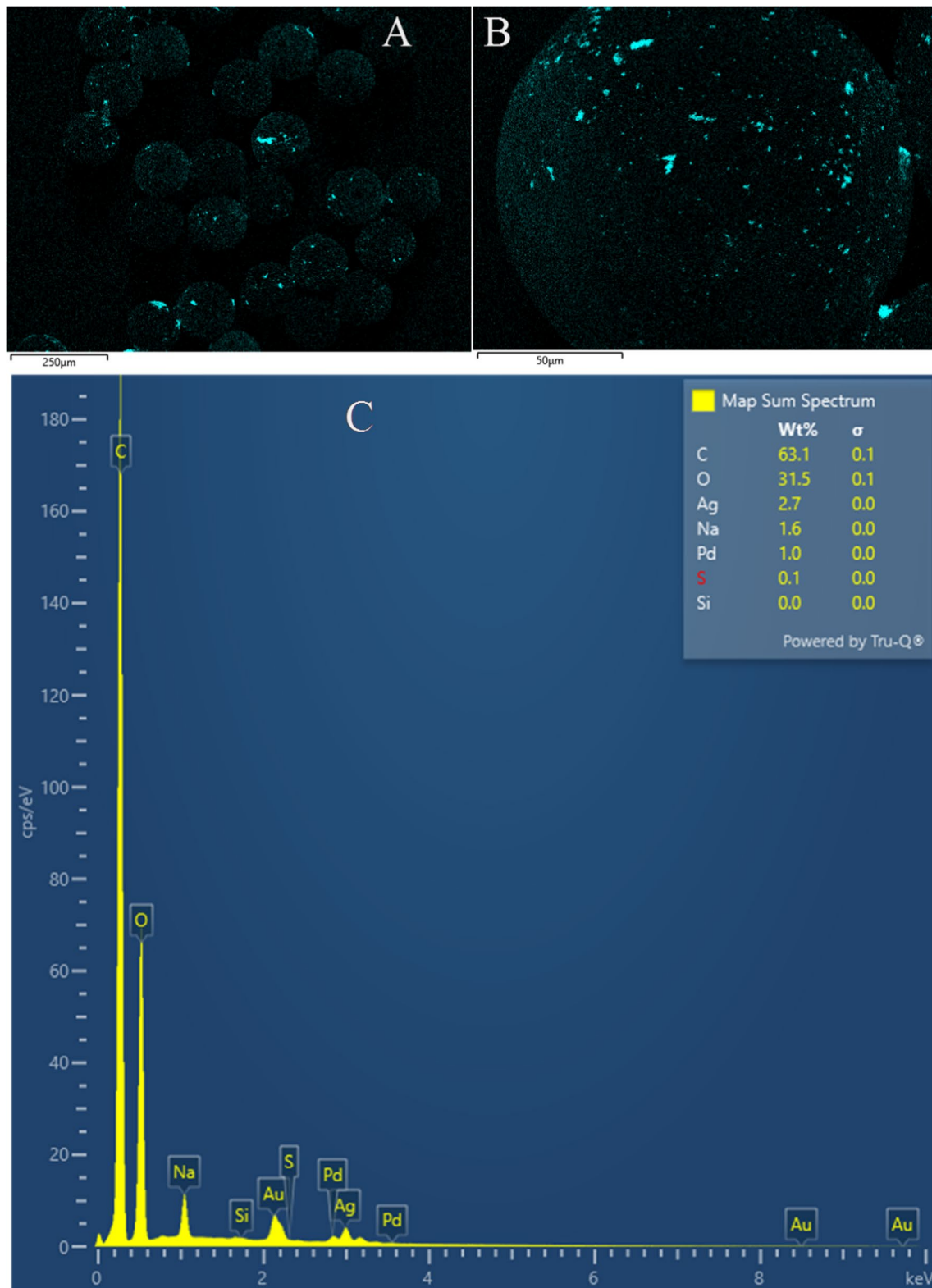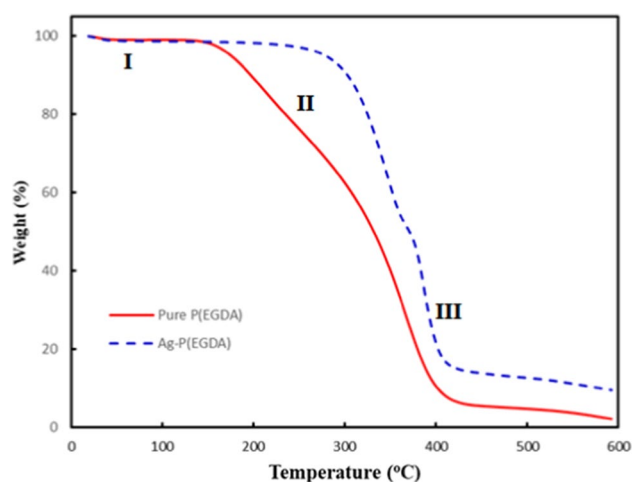
Fig. 5 **A** and **B** Energy-dispersive X-ray (EDX) silver mapping of Ag–P(EGDA) beads at two different magnifications and **C** EDX spectra over the selected area
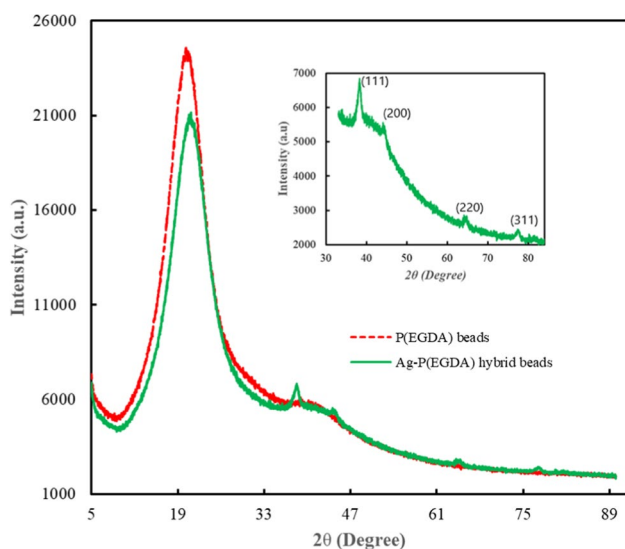
Fig. 6 XRD analysis of P(EGDA) microgels (red dotted line) and Ag–P(EGDA) hybrid microgels (green solid line). Inset gives the XRD of Ag–P(EGDA) hybrid beads in 2θ range of 30–84°

Fig. 7 Thermogravimetric analysis of P(EGDA) microgels and Ag–P(EGDA) hybrid microgels

temperatures, Fig. 7. This observation may be attributed to the reduction in polymer chain mobility due to presence of silver NPs in the polymeric network. In Region III (T > 320 °C for pure beads and T > 380 °C for composite beads), degradation of polymer backbone (C–C) bonds may be the main reason for accelerated weight loss. Polymeric material was completely degraded at about 430 °C in both cases. Our results are in good agreement with previously reported TGA results of P(EGDA) beads and polydopamine-P(EGDA) hybrid beads [19]. The residual mass difference between P(EGDA) and Ag–P(EGDA) microgels at $T = 592$ °C roughly corresponds to the weight percentage of silver

in the hybrid beads and was found to be 7.4%. The results of the TGA analysis confirm that silver NPs were successfully loaded into P(EGDA) beads and that the Ag–P(EGDA) beads can be used over a wide range of temperatures without degradation of polymeric support.

3.2 Catalytic activity of Ag–P(EGDA) hybrid beads

3.2.1 Reduction of 4-nitrophenol using Ag–P(EGDA)

The reduction of 4-nitrophenol into 4-aminophenol with NaBH$_4$ will be used as one of the model reactions to test the catalytic action of Ag–P(EGDA) hybrid beads. The choice of this reaction to check the catalytic potential of Ag–P(EGDA) hybrid beads was based on several reasons. First of all, 4-nitrophenol is a toxic substance which is present in wastewater generated from different industries, while its reduction product (4-aminophenol) has low toxicity and is a valuable chemical reagent required for various industrial processes, for example in pharmaceutical, textile, and agrochemical industry [43, 44]. 4-nitrophenol is soluble in water and causes significant toxic effects on aquatic life [45, 46]. Therefore, its conversion into 4-aminophenol is of high importance in pollution control and many industrial processes. Sodium borohydride cannot reduce 4-nitrophenol without a catalyst. However, 4-nitrophenol can be successfully converted into 4AP using NaBH$_4$ as a reductant in the presence of zerovalent metal nanoparticles [47–50]. Furthermore, the progress of the reduction of 4NP into 4AP can easily be monitored by a widely available technique (UV–visible spectrophotometry). Finally, the reaction can be performed at ambient temperature in water, which is the greenest and safest solvent. Therefore, the reduction of 4-nitrophenol into 4-aminophenol has turned out to be a yard stick to check the catalytic efficacy of metal nanoparticles [51–55].

Before testing composite beads as catalysts for the reduction of 4NP, it was important to check that P(EGDA) and Ag–P(EGDA) beads do not cause any interference with absorbance measurements at 300 nm and 400 nm. For this purpose, P(EGDA) and Ag–P(EGDA) beads (0.06 g each) were suspended separately in 22 mL of deionised water and stirred overnight before a UV–visible spectrum of the supernatant of each suspension was recorded at 240–800 nm. No peak was observed in this wavelength region (Fig. S2, Supporting Information) indicating that both P(EGDA) and Ag–P(EGDA) microgels do not release any substance that can interfere with absorbance peaks of 4NP and 4AP. Depending upon their size, silver NPs dispersed in aqueous media display surface plasmon resonance peaks in the wavelength range of 400–450 nm [8, 56, 57]. Therefore, silver NPs were tightly bound on P(EGDA) beads, and no leaching occurred during the prolonged stirring process.
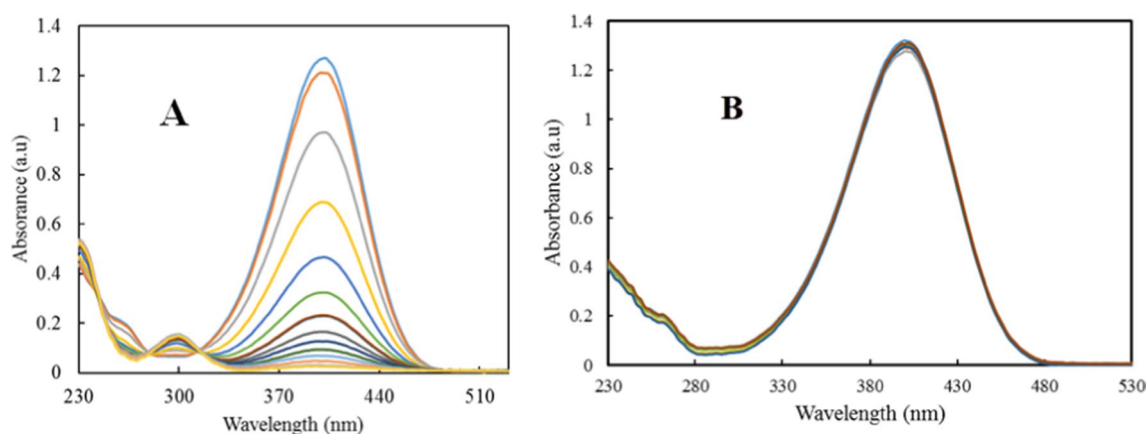
Fig. 8 A UV–visible spectra during reduction of 4-nitrophenol (0.08 mM) with NaBH$_4$ (8.33 mM) in water in the presence of Ag–P(EGDA) hybrid beads (2.08 mg/mL) at room temperature recorded at regular time intervals of 3 min. **B** UV–visible spectra during reduc-tion of 4NP (0.08 mM) with NaBH$_4$ (8.33 mM) in water at room temperature in the absence of Ag–P(EGDA) microgel particles over the same time interval

Therefore, the reduction of 4NP can be examined without any interference of the plasmonic band of silver NPs with the absorbance of 4-nitrophenolate ions.

The UV–visible spectra recorded during the Ag–P(EGDA) catalysed reduction of 4NP into 4AP in water at room temperature are shown in Fig. 8A.

A gradual drop in the height of the absorbance band at 400 nm (λ_{max} of 4NP under slightly basic conditions in aqueous solutions) and simultaneous increase in the height of absorbance peak at 300 nm (λ_{max} of 4AP) in the presence of Ag–P(EGDA) hybrid beads was a clear indication of the progressive conversion of 4NP to 4AP. The presence of two isosbestic points at 280 nm and 314 nm in the spectra shown in Fig. 8A shows that this is a genuine unimolecular reaction without any other side reactions [58, 59]. 4NP was completely converted into 4AP after 40 min. The progression of the reduction of 4NP into 4AP was also monitored under the same reaction conditions without using Ag–P(EGDA) hybrid beads, and the UV–vis spectra are shown in Fig. 8B. No decline in the height of the absorbance peak at 400 nm and no increase in absorbance at 300 nm was observed over 40 min, showing that the reduction of 4NP into 4AP was kinetically restricted in the absence of hybrid microgel particles.

The reduction of 4NP by NaBH$_4$ was also tried in the presence of P(EGDA) beads, but no change of absorbance at 400 nm was observed (Fig. S3, Supporting Information) indicating that pure P(EGDA) microgel does not have any catalytic activity. Moreover, it confirmed that the decline in absorbance at 400 nm in Fig. 8A was not due to the physical adsorption of 4NP onto the polymer beads. In another experiment, pure P(EGDA) beads were placed in a solution of 4NP to check if 4NP could be adsorbed on the beads in the absence of NaBH$_4$. In this case, one drop of 0.1 M NaOH was added to the mixture because 4NP shows a peak at 400 nm only under alkaline conditions [60]. No decrease in absorbance at 400 nm was observed over 140 min if the mixture was stirred overnight before the UV–vis measurements (Fig. S4, supporting information). However, if the UV/Vis spectra were recorded shortly after pH adjustment, the increase in absorbance at 270 and 400 nm was observed over time (Fig. S5, supporting information). It can be explained by the gradual shift of equilibrium between 4-nitrophenol and 4-nitrophenolate ions towards 4-nitrophenolate ion upon the addition of NaOH due to the increase of the pH over time. After overnight stirring, no significant increase in absorbance was observed over time, because the system has already achieved the equilibrium. Similarly, when Ag–P(EGDA) beads were placed in a basic 4NP solution in the absence of NaBH$_4$, no decline in absorbance at 400 nm as well as no rise in absorbance at 300 nm was observed (the data not provided here) which confirms that Ag–P(EGDA) beads have no reducing moieties.

The reaction kinetics of 4NP reduction was investigated based on the rate of disappearance of the absorbance peak at 400 nm. The reaction was carried out at [NaBH$_4$]/[4NP] $\geq$ 100 to satisfy the condition of pseudo-first-order kinetics that can be described by Eq. (1):

$$\ln \frac{A_t}{A_o} = -k_{app}t \tag{1}$$

The apparent rate constant (k_{app}) was evaluated from the gradient of the $\ln\left(A_t/A_o\right)$ vs. timeline, as shown in Fig. 9, where A_t and A_o are the absorbance values at λ_{max} of the reactant at any time t throughout the reaction and at zero time, respectively.
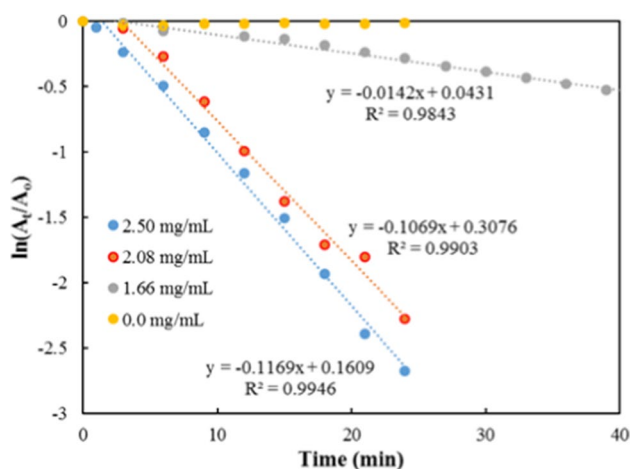
Fig. 9 Pseudo first-order kinetic fitting for the reduction of 4-nitrophenol (0.08 mM) by NaBH$_4$ (8.33 mM) at different loadings of Ag–P(EGDA) hybrid beads in the reaction mixture

Different amounts of Ag–P(EGDA) hybrid beads were added to the reaction mixture to study the effect of catalyst loading on the value of k_{app}. At the loading of catalytic beads of 1.66, 2.08, and 2.50 mg/mL, the k_{app} value for 4NP reduction was found to be 0.0142, 0.107, and 0.117 min^{-1}, respectively. A steady increase of k_{app} with an increase in Ag–P(EGDA) loading in the reaction mixture indicates that the reduction is occurring on the surface of the catalyst.

The mechanism of reduction of 4NP into 4AP by metal nanoparticles immobilised on different supports is well-established and has been described elsewhere [61, 62]. According to most of the studies, 4NP and reductant are both adsorbed on the surface of metal nanoparticles before the reaction and then 4NP is converted into 4AP on the surface of nanoparticles according to Langmuir–Hinshelwood modelling.

3.2.2 Ag–P(EGDA) catalysed reduction of methylene blue

Textile industrial waste effluents containing aromatic dyes have become a major source of water pollution on Earth [63, 64]. Methylene blue (MeB) is one of the major water pollutants, and its presence in water reduces the dissolution of oxygen and sunlight penetration which threatens aquatic life [65]. We have recently reviewed the degradation of MeB using various catalytic systems [66] and to the best of our knowledge, the degradation of MeB by Ag–P(EGDA) hybrid microgels has not yet been reported. Therefore, Ag–P(EGDA) beads were also tested as a catalyst for the degradation of MeB by NaBH$_4$ in water at 19 °C (Fig. 10).

First, the degradation of MeB by NaBH$_4$ using Ag–P(EGDA) as a catalyst was confirmed by naked-eye observation. At the loading of Ag–P(EGDA) of 2.0 mg/mL, the blue colour of the reaction mixture (25.0 μM MeB + 29.1 mM NaBH$_4$) disappeared within 6.0 min (inset of Fig. 10A). Then, MeB degradation was monitored quantitatively by UV–vis spectroscopy using the same catalyst and reactant concentrations to study the kinetics of the reaction. Figure 10A shows time-dependent UV–visible spectra of the reaction mixture. The peak absorbance at 664 nm decreased over time due to the degradation of MeB. Interestingly, the reaction was very fast, and the dye was completely degraded within 6 min, which indicates that Ag–P(EGDA) is an efficient catalyst for the degradation of organic dyes present in aqueous solutions at very low concentrations. Figure 10B shows time-dependent UV–vis spectra of the mixture of MeB and NaBH$_4$ without Ag–P(EGDA). The absorbance peak of MeB was stable and did not change in the time domain of 0–15 min showing that the dye could not be degraded by NaBH$_4$ without catalyst. The k_{app} value for the catalytic reduction of MeB by NaBH$_4$ in the presence of Ag–P(EGDA) was estimated from the gradient of
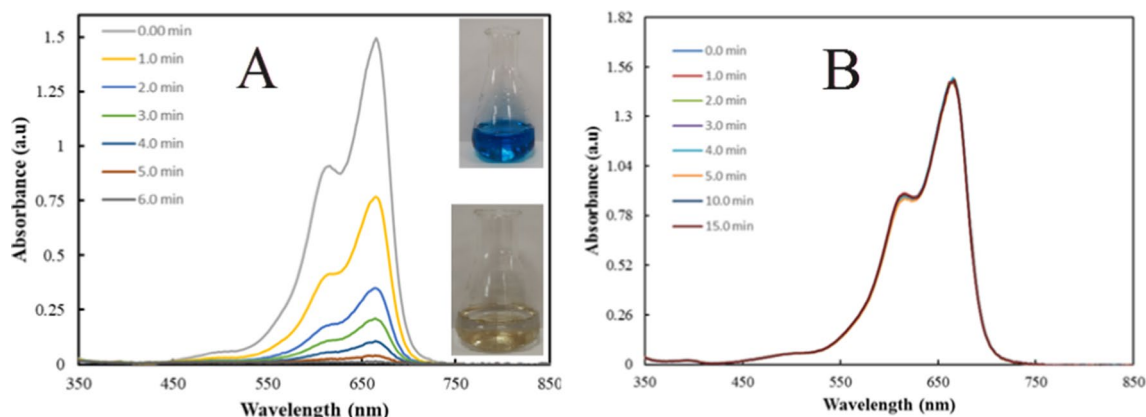
Fig. 10 Time-dependent UV–vis spectra of the mixture of MeB (25.0 μM) and NaBH$_4$ (29.1 mM) in the presence of Ag–P(EGDA) (2.0 mg/mL) (**A**) and in the absence of Ag–P(EGDA) (**B**). Inset images in **A** show the reaction mixture before and after reduction
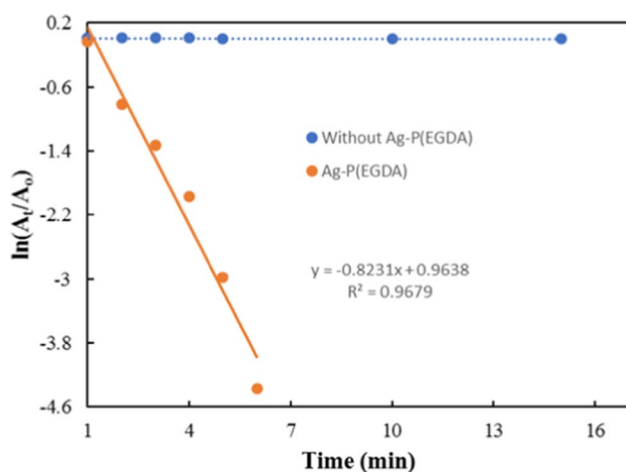
Fig. 11 Fitting the experimental data for the degradation of MeB (25.0 μM) by NaBH$_4$ (29.1 mM) in the presence of Ag–P(EGDA) (2.0 mg/mL) to the pseudo first-order kinetic model. The experimental data obtained without adding any catalyst are also shown

the $\ln\left(A_t/A_o\right)$ vs. t line, given in Fig. 11 and it was found to be 0.82 min^{-1}.

To check the applicability of Ag–P(EGDA) catalyst on an industrial scale, the reduction of MeB was performed using a recycled catalyst under the same reaction conditions. For this purpose, Ag–P(EGDA) was recovered from the reaction mixture and washed with water. The recovered catalyst was dried and then used for the next cycle. UV–vis spectra of MeB degradation using the recycled catalyst and the corresponding pseudo-first-order kinetics plot are given in Figures S6 and S7, respectively. It was observed that the Ag–P(EGDA) catalyst was still active after recycling but had slightly reduced activity. Using fresh catalyst, 99.4% of MeB was degraded in 6 min, and the recycled catalyst was able to degrade 96% of MeB in 18 min.

4 Conclusions

Monodisperse P(EGDA) microgel particles with wrinkled surfaces were successfully fabricated using a novel Lego-inspired droplet microfluidic device. In situ loading of silver nanoparticles in the cavities of crosslinked P(EGDA) polymer particles with the wrinkled surface was achieved by the reduction of AgNO$_3$ in an aqueous medium in the presence of P(EGDA) beads. TGA analysis revealed that the weight percentage of silver in the hybrid beads was 7.4%. Most of the silver nanoparticles are present on the surface of microgel particles, which means that internal mass transfer limitations of the hybrid beads during catalytic reactions can be neglected. The surface of P(EGDA) beads was smoother and less porous after the incorporation of silver NPs and offered better protection against water evaporation in TGA measurements compared to pristine polymer surfaces. Ag–P(EGDA) hybrid system showed excellent catalytic activity towards the reduction of 4NP and MeB from their aqueous solutions, and both reactions followed a pseudo-first-order kinetic model. We envision that the fabricated composite beads can be used to degrade other nitroarenes and toxic dyes. Ag–P(EGDA) system may find an important application in wound-healing scaffolds and coatings for implantable medical devices and contact lenses due to the potential antibacterial properties of silver NPs. A similar strategy applied here for the fabrication of Ag–P(EGDA) composite microgels can be used for the production of composite P(EGDA) microgels loaded with gold NPs and iron oxide NPs in the future. The Ag–P(EGDA) system has the potential to be used in antibacterial, antiviral, and antifungal functional materials, such as wound dressings, orthopaedic materials, vascular catheters, and tissue engineering scaffolds.

References

1. G. Agrawal, R. Agrawal, Functional microgels: recent advances in their biomedical applications. Small **14**(39), 1801724 (2018)

2. R. Begum, Z.H. Farooqi, S.R. Khan, Poly (N-isopropylacrylamide-acrylic acid) copolymer microgels for various applications: a review. Int. J. Polym. Mater. Polym. Biomater. **65**(16), 841–852 (2016)

3. A. Fernández-Barbero, I.J. Suárez, B. Sierra-Martín, A. Fernández-Nieves, F.J. de Las Nieves, M. Marquez, J. Rubio-Retama, E. López-Cabarcos, Gels and microgels for nanotechnological applications. Adv. Colloid Interface Sci. **147**, 88–108 (2009)

4. M. Arif, Z.H. Farooqi, A. Irfan, R. Begum, Gold nanoparticles and polymer microgels: last five years of their happy and successful marriage. J. Mol. Liq. **336**, 116270 (2021)

5. J. Zhang, S. Xu, E. Kumacheva, Polymer microgels: reactors for semiconductor, metal, and magnetic nanoparticles. J. Am. Chem. Soc. **126**(25), 7908–7914 (2004)

6. M. Karg, A. Pich, T. Hellweg, T. Hoare, L.A. Lyon, J. Crassous, D. Suzuki, R.A. Gumerov, S. Schneider, I.I. Potemkin, Nanogels and microgels: from model colloids to applications, recent developments, and future trends. Langmuir **35**(19), 6231–6255 (2019)

7. Z. Mahdieh, A. Holian, Electrospun fibers loaded with ball-milled poly (n-isopropylacrylamide) microgel particles for smart delivery applications. J. Appl. Polym. Sci. **137**(44), 49786 (2020)

8. R. Begum, Z.H. Farooqi, A.H. Aboo, E. Ahmed, A. Sharif, J. Xiao, Reduction of nitroarenes catalyzed by microgel-stabilized silver nanoparticles. J. Hazard. Mater. **377**, 399–408 (2019)

9. K. Naseem, Z.H. Farooqi, R. Begum, M. Ghufran, M.Z.U. Rehman, J. Najeeb, A. Irfan, A.G. Al-Sehemi, Poly (N-isopropyl-methacrylamide-acrylic acid) microgels as adsorbent for removal of toxic dyes from aqueous medium. J. Mol. Liq. **268**, 229–238 (2018)

10. M. Kohestanian, H. Bouhendi, Novel cross-linking mechanism for producing PAA microgels synthesized by precipitation polymerization method. Colloid Polym. Sci. **293**, 1983–1995 (2015)

11. O. Virtanen, W. Richtering, Kinetics and particle size control in non-stirred precipitation polymerization of N-isopropylacrylamide. Colloid Polym. Sci. **292**, 1743–1756 (2014)

12. L.R. Kesselman, S. Shinwary, P.R. Selvaganapathy, T. Hoare, Synthesis of monodisperse, covalently cross-linked, degradable "smart" microgels using microfluidics. Small **8**(7), 1092–1098 (2012)

13. S. Seiffert, D.A. Weitz, Microfluidic fabrication of smart microgels from macromolecular precursors. Polymer **51**(25), 5883–5889 (2010)

14. L.Y. Chu, J.W. Kim, R.K. Shah, D.A. Weitz, Monodisperse thermoresponsive microgels with tunable volume-phase transition kinetics. Adv. Funct. Mater. **17**(17), 3499–3504 (2007)

15. B.K. Pullagura, S. Amarapalli, V. Gundabala, Coupling electrohydrodynamics with photopolymerization for microfluidics-based generation of polyethylene glycol diacrylate (PEGDA) microparticles and hydrogels. Colloids Surf. A **608**, 125586 (2021)

16. F. Sharifi, B.B. Patel, M.C. McNamara, P.J. Meis, M.N. Roghair, M. Lu, R. Montazami, D.S. Sakaguchi, N.N. Hashemi, Photo-cross-linked poly (ethylene glycol) diacrylate hydrogels: spherical microparticles to bow tie-shaped microfibers. ACS Appl. Mater. Interfaces **11**(20), 18797–18807 (2019)

17. X.Z. Zhang, C.C. Chu, Temperature-sensitive poly (N-isopropylacrylamide)/poly (ethylene glycol) diacrylate hydrogel microspheres. Am. J. Drug Delivery **3**(1), 55–65 (2005)

18. G. Celetti, C. Di Natale, F. Causa, E. Battista, P.A. Netti, Functionalized poly (ethylene glycol) diacrylate microgels by microfluidics: in situ peptide encapsulation for in serum selective protein detection. Colloids Surf. B **145**, 21–29 (2016)

19. H. Liu, X. Qian, Z. Wu, R. Yang, S. Sun, H. Ma, Microfluidic synthesis of QD-encoded PEGDA microspheres for suspension assay. J. Mater. Chem. B **4**(3), 482–488 (2016)

20. C.L. Lewis, Y. Lin, C. Yang, A.K. Manocchi, K.P. Yuet, P.S. Doyle, H. Yi, Microfluidic fabrication of hydrogel microparticles containing functionalized viral nanotemplates. Langmuir **26**(16), 13436–13441 (2010)

21. K.K. Kang, K. Shim, C.S. Lee, Immobilization of physicochemically stable Pd nanocatalysts inside uniform hydrogel microparticles. Colloids Surf. A **593**, 124607 (2020)

22. D.J. Kim, T.Y. Jeon, S.G. Park, H.J. Han, S.H. Im, D.H. Kim, S.H. Kim, Uniform microgels containing agglomerates of silver nanocubes for molecular size-selectivity and high SERS activity. Small **13**(23), 1604048 (2017)

23. F.M. Aldakheel, D. Mohsen, M.M. El Sayed, K.A. Alawam, A.S. Binshaya, S.A. Alduraywish, Silver nanoparticles loaded on chitosan-g-PVA hydrogel for the wound-healing applications. Molecules **28**(7), 3241 (2023)

24. A. Ahsan, M.A. Farooq, Therapeutic potential of green synthesized silver nanoparticles loaded PVA hydrogel patches for wound healing. J. Drug Deliv. Sci. Technol. **54**, 101308 (2019)

25. H. Pangli, S. Vatanpour, S. Hortamani, R. Jalili, A. Ghahary, Incorporation of silver nanoparticles in hydrogel matrices for controlling wound infection. J. Burn Care Res. **42**(4), 785–793 (2021)

26. F.M. Aldakheel, M.M.E. Sayed, D. Mohsen, M.H. Fagir, D.K. El Dein, Green synthesis of silver nanoparticles loaded hydrogel for wound healing; systematic review. Gels **9**(7), 530 (2023)

27. Q. Dong, D. Zu, L. Kong, S. Chen, J. Yao, J. Lin, L. Lu, B. Wu, B. Fang, Construction of antibacterial nano-silver embedded bioactive hydrogel to repair infectious skin defects. Biomater. Res. **26**(1), 36 (2022)

28. M. Zakia, J.M. Koo, D. Kim, K. Ji, P. Huh, J. Yoon, S.I. Yoo, Development of silver nanoparticle-based hydrogel composites for antimicrobial activity. Green Chem. Lett. Rev. **13**(1), 34–40 (2020)

29. J. Chen, F. Chen, Y. Wang, M. Wang, Q. Wu, X. Zhou, X. Ge, One-step synthesis of poly (ethyleneglycol dimethacrylate)-microspheres-supported nano-Au catalyst in methanol–water solution under γ-ray radiation. RSC adv. **6**(61), 55878–55883 (2016)

30. R. Begum, K. Naseem, Z.H. Farooqi, A review of responsive hybrid microgels fabricated with silver nanoparticles: synthesis, classification, characterization and applications. J. Sol-Gel Sci. Technol. **77**(2), 497–515 (2016)

31. M.V. Bandulasena, G.T. Vladisavljević, B. Benyahia, Versatile reconfigurable glass capillary microfluidic devices with Lego® inspired blocks for drop generation and micromixing. J. Colloid Interface Sci. **542**, 23–32 (2019)

32. M. Chen, R. Aluunmani, G. Bolognesi, G.T. Vladisavljević, Facile microfluidic fabrication of biocompatible hydrogel microspheres in a novel microfluidic device. Molecules **27**(13), 4013 (2022)

33. M. Chen, Z.H. Farooqi, G. Bolognesi, G.T. Vladisavljević, Microfluidic fabrication of monodisperse and recyclable TiO_2-poly (ethylene glycol) diacrylate hybrid microgels for removal of methylene blue from aqueous medium. Langmuir **39**(51), 18784–18796 (2023)

34. M. Choi, M. Humar, S. Kim, S.H. Yun, Step-index optical fiber made of biocompatible hydrogels. Adv. Mater. **27**(27), 4081–4086 (2015)

35. C. Charton, P. Colon, F. Pla, Shrinkage stress in light-cured composite resins: influence of material and photoactivation mode. Dent. mater. **23**(8), 911–920 (2007)

36. A. Peutzfeldt, Resin composites in dentistry: the monomer systems. Eur. J. Oral Sci. **105**(2), 97–116 (1997)

37. G.M. Cruise, D.S. Scharp, J.A. Hubbell, Characterization of permeability and network structure of interfacially photopolymerized poly (ethylene glycol) diacrylate hydrogels. Biomaterials **19**(14), 1287–1294 (1998)

38. E.E. Ekanem, S.A. Nabavi, G.T. Vladisavljević, S. Gu, Structured biodegradable polymeric microparticles for drug delivery produced using flow focusing glass microfluidic devices. ACS Appl. Mater. Interfaces **7**(41), 23132–23143 (2015)

39. J. Kim, J. Joo, S.Y. Park, Preparation of asymmetric porous Janus particles using microfluidics and directional UV curing. Part. Part. Syst. Charact. **30**(11), 981–988 (2013)

40. Y. Dong, Y. Ma, T. Zhai, F. Shen, Y. Zeng, H. Fu, J. Yao, Silver nanoparticles stabilized by thermoresponsive microgel particles: synthesis and evidence of an electron donor-acceptor effect. Macromol. Rapid Commun. **28**(24), 2339–2345 (2007)

41. A. Irzh, N. Perkas, A. Gedanken, Microwave-assisted coating of PMMA beads by silver nanoparticles. Langmuir **23**(19), 9891–9897 (2007)

42. K. Kim, H.B. Lee, H.K. Park, K.S. Shin, Easy deposition of Ag onto polystyrene beads for developing surface-enhanced-Raman-scattering-based molecular sensors. J. Colloid Interface Sci. **318**(2), 195–201 (2008)

43. N. Wang, F. Wang, F. Pan, S. Yu, D. Pan, Highly efficient silver catalyst supported by a spherical covalent organic framework for the continuous reduction of 4-nitrophenol. ACS Appl. Mater. Interfaces **13**(2), 3209–3220 (2021)

44. W. Jia, F. Tian, M. Zhang, X. Li, S. Ye, Y. Ma, W. Wang, Y. Zhang, C. Meng, G. Zeng, Nitrogen-doped porous carbon-encapsulated copper composite for efficient reduction of 4-nitrophenol. J. Colloid Interface Sci. **594**, 254–264 (2021)

45. M. Teimouri, F. Khosravi-Nejad, F. Attar, A.A. Saboury, I. Kostova, G. Benelli, M. Falahati, Gold nanoparticles fabrication by plant extracts: synthesis, characterization, degradation of 4-nitrophenol from industrial wastewater, and insecticidal activity–a review. J. Cleaner Prod. **184**, 740–753 (2018)

46. P. Balasubramanian, T. Balamurugan, S.M. Chen, T.W. Chen, Simplistic synthesis of ultrafine $CoMnO_3$ nanosheets: an excellent electrocatalyst for highly sensitive detection of toxic 4-nitrophenol in environmental water samples. J. Hazard. Mater. **361**, 123–133 (2019)

47. Z. Chen, K. Leng, X. Zhao, S. Malkhandi, W. Tang, B. Tian, L. Dong, L. Zheng, M. Lin, B.S. Yeo, Interface confined hydrogen evolution reaction in zero valent metal nanoparticles-intercalated molybdenum disulfide. Nat. Commun. **8**(1), 1–9 (2017)

48. S. Bae, S. Gim, H. Kim, K. Hanna, Effect of $NaBH_4$ on properties of nanoscale zero-valent iron and its catalytic activity for reduction of p-nitrophenol. Appl. Catal. B **182**, 541–549 (2016)

49. F.U. Khan, S.B. Khan, T. Kamal, A.M. Asiri, I.U. Khan, K. Akhtar, Novel combination of zero-valent Cu and Ag nanoparticles@ cellulose acetate nanocomposite for the reduction of 4-nitrophenol. Int. J. Biol. Macromol. **102**, 868–877 (2017)

50. S. Liu, Y. Guo, S. Yi, S. Yan, C. Ouyang, F. Deng, C. Li, G. Liao, Q. Li, Facile synthesis of pure silicon zeolite-confined silver nanoparticles and their catalytic activity for the reduction of 4-nitrophenol and methylene blue. Sep. Purif. Technol. **307**, 122727 (2023)

51. K. Kuroda, T. Ishida, M. Haruta, Reduction of 4-nitrophenol to 4-aminophenol over Au nanoparticles deposited on PMMA. J. Mol. Catal. A: Chem. **298**(1–2), 7–11 (2009)

52. J. Strachan, C. Barnett, A.F. Masters, T. Maschmeyer, 4-Nitrophenol reduction: probing the putative mechanism of the model reaction. ACS Catal. **10**(10), 5516–5521 (2020)

53. Y.R. Mejía, N.K.R. Bogireddy, Reduction of 4-nitrophenol using green-fabricated metal nanoparticles. RSC adv. **12**(29), 18661–18675 (2022)

54. Z.S. Lv, X.Y. Zhu, H.B. Meng, J.J. Feng, A.J. Wang, One-pot synthesis of highly branched Pt@ Ag core-shell nanoparticles as a recyclable catalyst with dramatically boosting the catalytic performance for 4-nitrophenol reduction. J. Colloid Interface Sci. **538**, 349–356 (2019)

55. J.A.E. Jacob, R. Antony, D.I. Jebakumar, Synergistic effect of silver nanoparticle-embedded calcite-rich biochar derived from Tamarindus indica bark on 4-nitrophenol reduction. Chemosphere **349**, 140765 (2024)

56. H. Veisi, S. Azizi, P. Mohammadi, Green synthesis of the silver nanoparticles mediated by Thymbra spicata extract and its application as a heterogeneous and recyclable nanocatalyst for catalytic reduction of a variety of dyes in water. J. Cleaner Prod. **170**, 1536–1543 (2018)

57. S. Iqbal, C. Zahoor, S. Musaddiq, M. Hussain, R. Begum, A. Irfan, M. Azam, Z.H. Farooqi, Silver nanoparticles stabilized in polymer hydrogels for catalytic degradation of azo dyes. Ecotoxicol. Environ. Saf. **202**, 110924 (2020)

58. P.T. Huang, Y.N. Chen, K.C. Chen, S.H. Wu, C.P. Liu, Confinement of silver nanoparticles in polystyrenes through molecular entanglements and their application for catalytic reduction of 4-nitrophenol. J. Mater. Chem. A **7**(36), 20919–20925 (2019)

59. S. Wunder, F. Polzer, Y. Lu, Y. Mei, M. Ballauff, Kinetic analysis of catalytic reduction of 4-nitrophenol by metallic nanoparticles immobilized in spherical polyelectrolyte brushes. J. Phys. Chem. C **114**(19), 8814–8820 (2010)

60. S. Saire-Saire, E.C. Barbosa, D. Garcia, L.H. Andrade, S. Garcia-Segura, P.H. Camargo, H. Alarcon, Green synthesis of Au decorated $CoFe_2O_4$ nanoparticles for catalytic reduction of 4-nitrophenol and dimethylphenylsilane oxidation. RSC adv. **9**(38), 22116–22123 (2019)

61. I. Hussain, Z.H. Farooqi, F. Ali, R. Begum, A. Irfan, W. Wu, X. Wang, M. Shahid, J. Nisar, Poly (styrene@ N-isopropylmethacrylamide-co-methacrylic acid)@ Ag hybrid particles with excellent catalytic potential. J. Mol. Liq. **335**, 116106 (2021)

62. M. Arif, M. Shahid, A. Irfan, J. Nisar, W. Wu, Z.H. Farooqi, R. Begum, Polymer microgels for the stabilization of gold nanoparticles and their application in the catalytic reduction of nitroarenes in aqueous media. RSC adv. **12**(9), 5105–5117 (2022)

63. R. Kishor, D. Purchase, G.D. Saratale, R.G. Saratale, L.F.R. Ferreira, M. Bilal, R. Chandra, R.N. Bharagava, Ecotoxicological and health concerns of persistent coloring pollutants of textile industry wastewater and treatment approaches for environmental safety. J. Environ. Chem. Eng. **9**(2), 105012 (2021)

64. A. Tkaczyk, K. Mitrowska, A. Posyniak, Synthetic organic dyes as contaminants of the aquatic environment and their implications for ecosystems: a review. Sci. Total Environ. **717**, 137222 (2020)

65. A.K. Moorthy, B.G. Rathi, S.P. Shukla, K. Kumar, V.S. Bharti, Acute toxicity of textile dye methylene blue on growth and metabolism of selected freshwater microalgae. Environ. Toxicol. Pharmacol. **82**, 103552 (2021)

66. R. Begum, J. Najeeb, A. Sattar, K. Naseem, A. Irfan, A.G. Al-Sehemi, Z.H. Farooqi, Chemical reduction of methylene blue in the presence of nanocatalysts: a critical review. Rev. Chem. Eng. **36**(6), 749–770 (2020)